J Physiol 587.6 (2009) pp 1187–1200

The Journal of Physiology

The spatial pattern of exocytosis and post-exocytic mobility of synaptopHluorin in mouse motor nerve terminals

Michael A. Gaffield[1], Lucia Tabares[2] and William J. Betz[1]

[1]*Department of Physiology and Biophysics, University of Colorado Denver, Anschutz Medical Campus, Aurora, CO 80045, USA*
[2]*Department of Medical Physiology and Biophysics, School of Medicine, University of Seville, 41009 Seville, Spain*

We monitored the spatial distribution of exo- and endocytosis at 37°C in mouse motor nerve terminals expressing synaptopHluorin (spH), confirming and extending earlier work at room temperature, which had revealed fluorescent 'hot spots' appearing in repeatable locations during tetanic stimulation. We also tested whether hot spots appeared during mild stimulation. Averaged responses from single shocks showed a clear fluorescence jump, but revealed no sign of hot spots; instead, fluorescence rose uniformly across the terminal. Only after 5–25 stimuli given at high frequency did hot spots appear, suggesting a novel initiation mechanism. Experiments showed that about half of the surface spH molecules were mobile, and that spH movement occurred out of hot spots, demonstrating their origin as exocytic sources, not endocytic sinks. Taken together, our results suggest that synaptic vesicles exocytose equally throughout the terminal with mild stimulation, but preferentially exocytose at specific, repeatable locations during tetanic stimulation.

(Received 19 November 2008; accepted after revision 14 January 2009; first published online 19 January 2009)
Corresponding author W. J. Betz: Department of Physiology and Biophysics, University of Colorado Denver, Anschutz Medical Campus, Aurora, CO 80045, USA. Email: bill.betz@uchsc.edu

A mouse motor nerve terminal presynaptic membrane contacts about 320 μm^2 of muscle fibre (Wood & Slater, 2001). With about 2.5 exocytic active zones per μm^2 of contact area (Fukunaga *et al.* 1983; Fukuoka *et al.* 1987), each terminal contains about 800 active zones in total. Little is currently known about the spatial distribution of synaptic vesicle exo- and endocytic events in the terminal during nerve activity. Studies of transgenic mice expressing the pH-sensitive exocytosis reporter synaptopHluorin (spH; Miesenbock *et al.* 1998) have revealed the appearance of discrete, reproducible spH fluorescent 'hot spots' (each several μm^2 in extent) during high frequency stimulation (Tabares *et al.* 2007; Wyatt & Balice-Gordon, 2008), which coincided with synaptic vesicle cluster locations (Wyatt & Balice-Gordon, 2008). However, all of these experiments were performed at room temperature. Exocytic rates (Micheva & Smith, 2005; Yang *et al.* 2005; Kushmerick *et al.* 2006; Gaffield & Betz, 2007; but see Fernandez-Alfonso & Ryan, 2004) and endocytic rates (Renden & von Gersdorff, 2007; Balaji *et al.* 2008), both of which may be involved in hot spot formation, increase substantially with increasing temperature. Additionally, synaptic vesicles are immobile at room temperature, but highly mobile at physiological temperature (Gaffield & Betz, 2007); therefore, we wondered whether hot spots might be less evident, less consistent, or disappear altogether at 37°C as synaptic vesicle diffusion and mixing become more pronounced.

Here, we report that hot spots are as evident at physiological temperature as at room temperature. We also extended these studies to fewer stimuli, to see, for example, whether repeated single stimuli (each of which evokes exocytosis of 50–70 quanta; Katz *et al.* 1997; Gaffield & Betz, 2007) reuse the same fusion sites. Our evidence suggests that these stimuli do not, but rather draw equally from fusion sites throughout the terminal. Only after between five and 25 stimuli at high frequency do hot spots emerge. Finally, we addressed the nature of the hot spots, that is, whether they are sites of increased exocytosis or endocytosis (cf. Teng *et al.* 1999; Teng & Wilkinson, 2000). After stimulation ceased, our experiments showed spH moving out of, not into, hot spots, revealing their probable exocytic origin.

Methods

Acute muscle preparation

spH mice (Tabares *et al.* 2007) were housed, handled and bred in accordance with the University of Colorado Denver

DOI: 10.1113/jphysiol.2008.166728

Institutional Animal Care and Use Committee. Animals were killed by halothane inhalation followed by cervical dislocation. The levator auris longus muscle was dissected from adult mice as described (Angaut-Petit *et al.* 1987) and pinned in a Sylgard-lined chamber. For stimulation of exocytosis, the nerve was drawn into a suction electrode. The perfusing solution contained (in mM): 137 NaCl, 5 KCl, 1.8 $CaCl_2$, 1 $MgSO_4$, 12 $NaHCO_3$, 1 NaH_2PO_4, and 11 glucose, pH 7.4, bubbled with 95% O_2–5% CO_2. During experiments, gravity fed perfusion was maintained at a rate of $\sim$1 ml min^{-1} into a volume of $\sim$5 ml. Temperature was maintained at $36 \pm 1^{\circ}$C using a dish heater DH-35 and inline heater SF-28 controlled and monitored by a dual automatic temperature controller TC-344B, all from Warner Instruments (Hamden, CT, USA). Muscle contraction was blocked by adding 3 μM curare (Sigma, St Louis, MO, USA).

Imaging and stimulation

Most imaging was performed on a Leica (Wetzlar, Germany) DM 4000B microscope with a Leica EL 6000 light source, a Leica L5 filtercube (BP 480/40 excitation, 505 dichroic, and BP 527/30) and a 63×, 0.9 NA water immersion objective from Zeiss (Oberkochen, Germany). Images were collected using an Andor (Belfast, UK) iXon EM+ DU-897E camera cooled to -55°C and controlled using Andor's Solis software, version 4.6.5. Pixels were 2×2 binned in the camera resulting in images with 270 nm pixels. For nerve stimulation, trains were generated using an A310 Accupulser and delivered using an A365 Stimulus Isolator, both from World Precision Instruments (Sarasota, FL, USA). Pulse durations were 500 μs. Precise timing control between imaging and stimulation was directed from software custom written in Matlab (The Mathworks, Natick, MA, USA) and sent to the instrumentation via a DAQ Card 6036E and a BNC-2090 board, both from National Instruments (Austin, TX, USA). For each stimulation the initial pulse was delivered 4–6 ms after the shutter opened for image acquisition. For single shock experiments, this means that a pulse was consistently delivered at about 5 ms into each stimulation frame (frames were 250 ms in duration).

For single shock experiments, to maximize signal to noise the light source was used at full strength, which resulted in lower noise and considerable photobleaching of surface spH (see Fig. 3*A*). Exposure times were typically 250 ms (selected to produce a clear signal when 100 responses to single shocks were averaged), which produced Gaussian noise of about 65 a.u. We estimated our best case single vesicle signal as follows. A single shock produced, on average, an increase of about 0.04% averaged over the entire terminal, which typically comprised about 4360 pixels with an average fluorescence of about 775 a.u. By multiplying these three values (0.0004, 4360 pixels, and 775 a.u. pixel^{-1}) we obtained an average total fluorescence change of around 1350 a.u. for a single shock. If we assume that the fluorescence arose from 70 distinct sites (1 site per quantum released by a single shock), each centered within one pixel, then the signal would be about 20 a.u. per release site. However, based on the measured diffusion coefficient (Fig. 5), about half of the spH can move up to several diffraction limited pixels ($\sim$700 nm) during the 250 ms frame capture time, making the expected signal closer to 10 a.u. Under our experimental conditions, constraining the fluorescence from single release events to within one pixel would require a substantial increase in frame rate, for example to video rate. This would limit spH movement between frames, but would also necessitate a much larger signal due to the shorter integration times. In summary, under our best case conditions, our single fusion signal-to-noise was about 10 : 65.

Image analysis

All image analysis was done using custom written Matlab programs. Most image series required some alignment (both by eye and automatically using least squares) before analysis. Any remaining misalignment never exceeded 1 pixel. Terminals were masked with hand drawn terminal boundaries. Due to small deviations in alignment, a 3×3 Gaussian smooth was performed before pixels were separated into deciles on the basis of fluorescence intensity. Decile binning was determined based on the total number of frames that each pixel showed a significant increase in spH intensity (2 standard deviations above control pixel fluctuation), in order to base deciles on fluorescence changes throughout the train. The pixels composing each decile were then used to determine fluorescence changes in *non-smoothed* data. For low shock data, the average response amplitude to a single shock or five shocks (data in Fig. 3*E*–*G*) was calculated after correcting for photobleaching and any uncompleted endocytosis and reacidification resulting from the previous stimulation six frames earlier. Both corrections were made simultaneously by subtracting a linear fit to the five control frames preceding each stimulation frame. In order to measure the time course of endocytosis and reacidification, we subtracted an 11-frame moving average from the raw data to correct for photobleaching alone. The resulting data (plotted in Fig. 3*C*) revealed a clear recovery phase with a time course much faster than the photobleaching. For identification of 'hot pixels', each pixel was smoothed with a 7×7 bin (centre pixel value set as average of all pixels in the bin). This large binning was chosen based on the distance spH was expected to move away from a central pixel in one frame (0.25 s), roughly three pixels in any direction (calculated from FRAP data; Fig. 5). This binning

allowed for complete capture of added fluorescence between frames. Each pixel was independently corrected for photobleaching before positive slopes were counted. Half-times of spH endocytosis and reacidification plotted in Fig. 6 were calculated using single exponential fits.

FRAP and modelling

FRAP imaging was performed on a Zeiss 510 laser scanning confocal microscope as described previously (Gaffield *et al.* 2006) using a 2 Hz imaging rate. A single ~2.25 μm diameter circle was bleached per trial. For resting terminals, the mobile fraction was calculated as the ratio of the actual recovery (as determined by the plateau reached at the end of recovery) to the total amount bleached. Autofluorescence due to the underlying muscle contributed ~9% of the total fluorescence. The amount of autofluorescence was not correlated with the mobile fraction from trial to trial; therefore, we assumed its contribution was minimal and excluded it from our analysis. Our earlier work showed that intraterminal vesicular spH was not bleached during FRAP experiments (Tabares *et al.* 2007), and thus we could assume that any mobile fraction was predominantly surface spH. The time course of recovery was calculated using a single exponential fit to the postbleach data. Fluorescence intensity as a function of time for FRAP of stimulated terminals (Fig. 5*B*) can be predicted by:

$$F(t) = f_m(F_s - F_o)(1 - e^{-t/\tau_{DIFF}}) + F_o + \frac{F_s - F_e}{F_s}[f_m(F_s - F_o) + F_o](e^{-t/\tau_{ENDO}} - 1) \quad (1)$$

where f_m is the mobile fraction, F_s is the fluorescence intensity in the unbleached region at the end of stimulation, F_o is the fluorescence intensity in the bleached region immediately after the bleach, F_e is the fluorescence intensity in the unbleached region after completion of endocytosis and reacidification (F_s, F_o and F_e are marked in Fig. 5*B*), τ_{DIFF} is the time constant of spH diffusion (from resting surface mobility), and τ_{ENDO} is the time constant of endocytosis and reacidification in the unbleached region. To model the expected recovery for various mobile fractions for the added spH (Fig. 5*C*), eqn (1) was separated into two different components, the initial surface spH and the added spH, which were subsequently summed. The variables F_s, F_o and F_e were scaled based on the relative fluorescence contributions of surface and added spH to the total. The mobile fraction, f_m, was kept at 0.41 for the initial surface spH, and varied for the added spH. To model the expected recovery for different uptake for mobile and immobile components (Fig. 5*D*), the surface and added spH components were separated into mobile and immobile components. For the surface, the mobile fraction was 41% of the total surface fluorescence while the added mobile fraction was set to 60% of the added fluorescence (based on the best fit from Fig. 5*C*). Next, the fluorescence endocytosed (reflected in the value $F_s - F_e$ in eqn (1)) was varied for the mobile and immobile components. Best fits for Fig. 5*C* and *D* were determined by eye.

Statistical analysis was performed using Microsoft Excel, and plots and curve fitting were done using Sigma Plot (Systat Software, San Jose, CA, USA). All experimental conditions were performed on at least three muscles from at least three different animals; trial numbers are listed in the figure legends. All error bars indicate standard error of the mean. Statistical difference was tested using the Student's t test with P values < 0.05 indicating significance.

Results

spH hot spots are stable and appear early during high frequency stimulation

Figure 1*A* (left panel) shows fluorescence hot spots immediately after tetanic stimulation (100 Hz for 30 s) at 37°C. After a 15 min rest, the tetanus was repeated, and again hot spots appeared (Fig. 1*A*, middle panel). Figure 1*A* (right panel) is an overlay; the largely yellow colour shows that the hot spots appeared at the same sites during each train. This is shown more quantitatively in Fig. 1*B*, which is a pixel-by-pixel comparison between the two trains. To facilitate comparisons amongst many different terminals (whose areas varied from 220 to 370 μm^2), we rank ordered all pixels according to amplitude of fluorescence change (ΔF), and then divided them into 10 equal-sized groups (deciles). Thus, the top (100%) decile included the pixels that responded the most during stimulation, while the 90% decile included the next 10%, and so on. Figure 1*C* shows the terminal pseudo-coloured according to these deciles. Figure 1*D* shows the magnitude of the fluorescence change in each decile. Note that a significant jump occurs in going to the top decile, which contains nearly one-third of the total fluorescence increase, reflecting pixels in the hot spots.

After sorting the first train into deciles, we could measure the fluorescence change in each of these deciles during subsequent trains of variable length to (1) see whether the top decile would continually respond more than the other deciles and (2) investigate how soon hot spots appear after the start of stimulation. Figure 2 shows that hot spots emerged as early as 25 shocks during the stimulus train. In each panel, we first determined as in Fig. 1*D* the ΔF decile for each pixel after a 30 s train (Train 1). The continuous lines show the ΔF values in each decile for train 1 for 25–3000 shocks. We then determined ΔF values for a second train (Train 2; also for 25–3000

shocks), assigning pixels according to the Train 1 deciles. The results (filled circles), agree well with the Train 1 data. In other words, the reproducible pattern of hot spots emerged after only a few hundred milliseconds of high frequency stimulation.

Hot spots do not predict release locations during mild stimulation

As shown in Fig. 3*A* (complete raw trace) and Fig. 3*B* (enlarged from box in 3*A*, after correction for photobleaching), we could not detect reliable fluorescence increases after a single shock to the nerve (each shock marked by a vertical line in Fig. 3*B*). However, if we averaged 100 responses to a single stimulus (given every 1.5 s), a clear signal emerged (Fig. 3*C*), even though it was less than 1% of the background fluorescence. In addition, we observed that the overall terminal response to 100 averaged single stimuli was diffuse and not spotty as with longer, high frequency trains (Fig. 3*D*). To quantify this difference, we binned pixels into deciles as before (according to ΔF after a 30 s train) and measured the average response to a single shock in each decile. The results (Fig. 3*E*, filled circles) showed that, while a clear overall response (upper dashed line) was evident, the response was produced evenly across all deciles. That is, the pixel locations that showed the largest ΔF after a 30 s train showed no such tendency after a single shock. The 10% decile did not show any change, nor did this decile change much with longer trains (see Fig. 2). We concluded

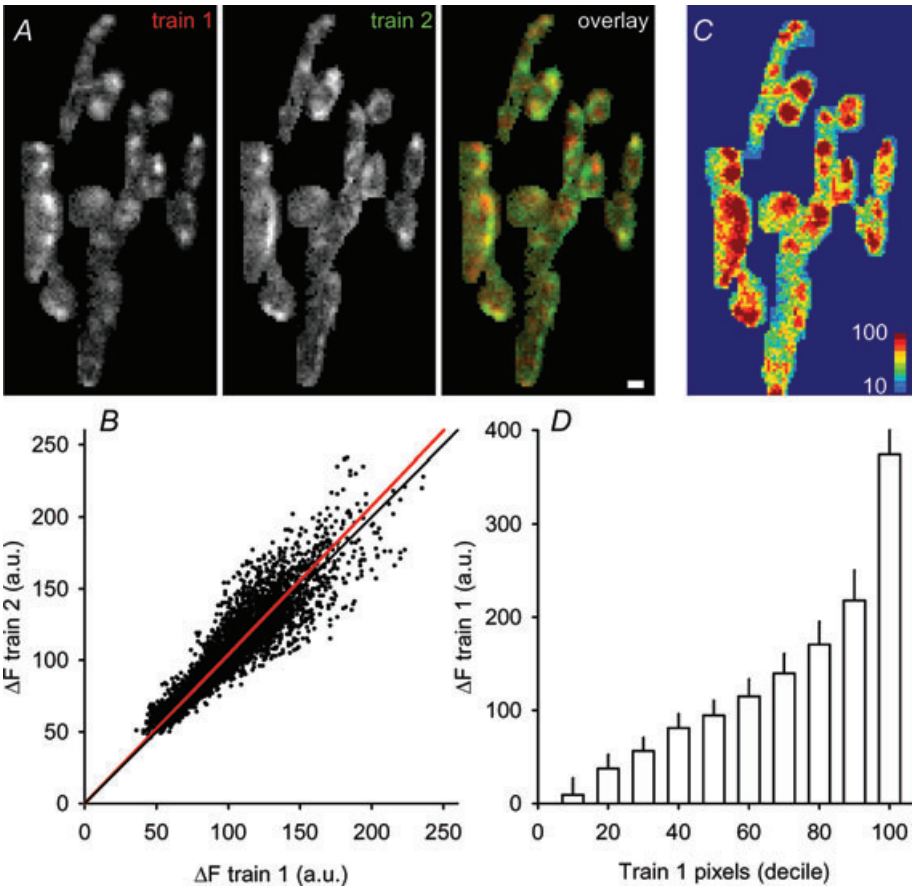

Figure 1. spH hot spots appear during prolonged stimulation
A, left, middle: masked intensity images showing spH difference levels after the end of a first and second 30 s, 100 Hz stimulation, respectively. Right: overlay for the two trials with train 1 pseudocoloured as red and train 2 pseudocoloured as green. Scale bar = 2 μm. *B*, correlation plot of fluorescence changes (in arbitrary units, a.u.). Train 1 (left panel in *A*) is plotted versus train 2 (middle panel in *A*) delivered 15 min later. The red line is a linear best fit with the intercept set to zero and a slope of 1.04; the black line is identity. *C*, same response to a train as shown in the left panel in *A*, but now coloured according to each pixel's relative spH intensity change. The top 10% of responding pixels are coloured in dark red (100), the next 10% in red, and so on for each decile down to 10 (indicated by colour bar). *D*, change in fluorescence is plotted for each decile. Fluorescence changed the most in the 100% decile, corresponding to the dark red pixels in panel *C*. $n = 12$ trials.

that this decile may have included some overestimation of the terminal boundary (selected by eye, see Methods), causing at least part of the 10% decile to exist outside of the terminal. Therefore, the 10% decile was excluded from future analysis.

To quantify fluorescence predictability, as shown in Fig. 3*F*, we compared the result from 100 single shocks at low frequency (filled circles, same data as Fig. 3*E*) with that obtained by giving 100 shocks at high frequency (continuous line), which predicted hot spot locations accurately. Clearly the single shock data (filled circles) fell closer to an even distribution (difference indicated by E) than to that predicted by the high frequency stimulation (difference indicated by P). A similar result was obtained with five stimuli (Fig. 3*G*). Finally, we calculated for all trains (1–3000 stimuli) a 'hot spot prediction factor' (Fig. 3*H*), based on a simple sum of squares (equation in Fig. 3*H* where E and P are as shown in Fig. 3*F*). The hot spot prediction curve in Fig. 3*H* shows a distinct threshold, with 1–5 shocks showing no hot spot predictive ability, but trains of 25–3000 stimuli showing excellent predictive ability. It thus appears that something happens between five and 25 stimuli at high frequency to 'turn on' hot spot locations. These results also suggest that hot spots do

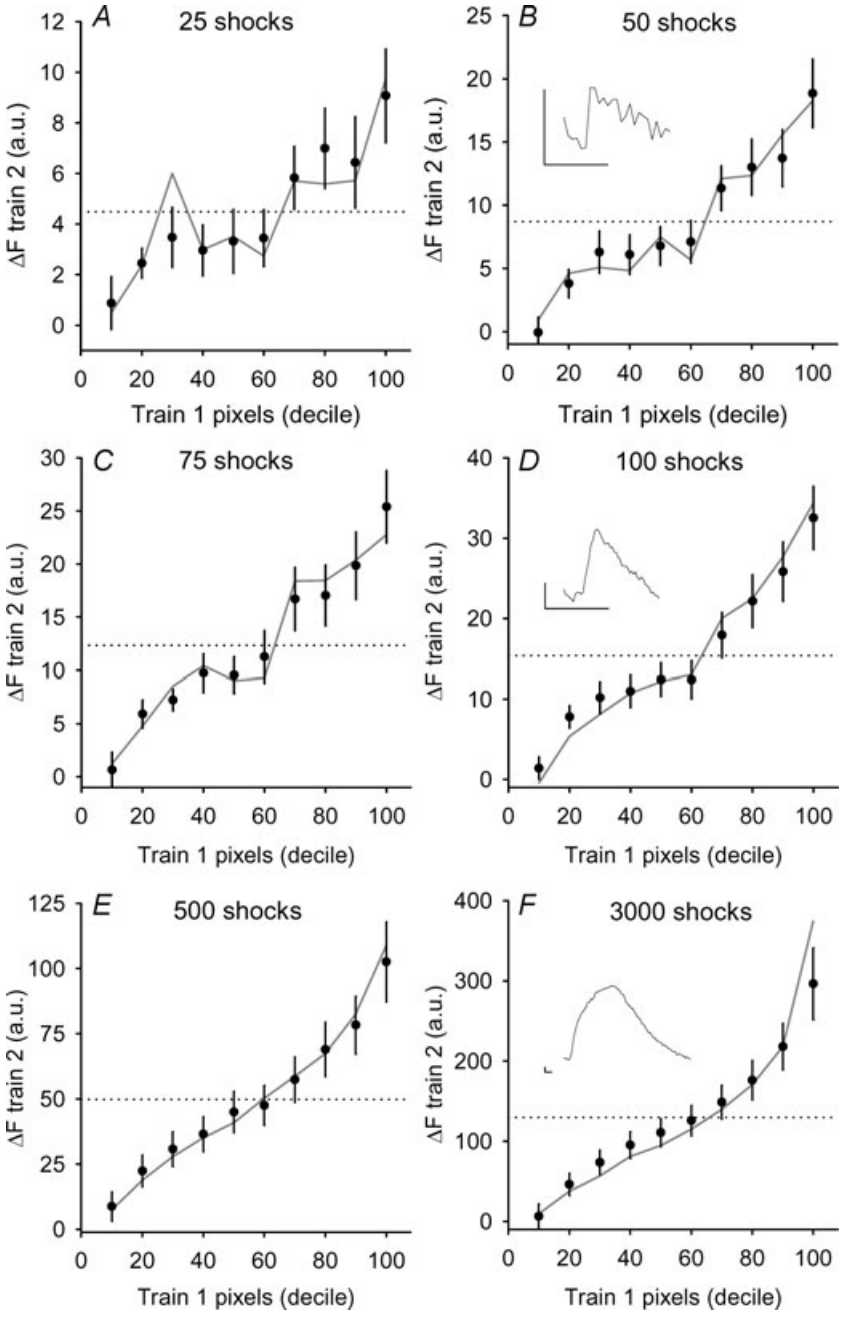

Figure 2. spH accumulates in predictable locations throughout high frequency trains
Pixels were separated into deciles based on spH fluorescence changes after a 30 s, 100 Hz stimulation (train 1). Those same locations were followed during a second, identical stimulation delivered 15 min later. Each plot shows the average change in spH fluorescence (arbitrary units, a.u.) in response to the second stimulation (train 2) after 25, 50, 75, 100, 500 and 3000 shocks (filled circles in *A*–*F*, respectively). For comparison, the fluorescence changes in response to train 1 for the same number of shocks are also plotted (grey lines), after normalizing to the overall slight difference in average fluorescence change in train 2 (dotted lines). $n = 16$ trials. Insets in *B*, *D* and *F*: examples of raw fluorescence traces averaged for a whole terminal stimulated just for the number of shocks listed. Vertical and horizontal scale lines indicate 10 a.u. and 5 s, respectively.

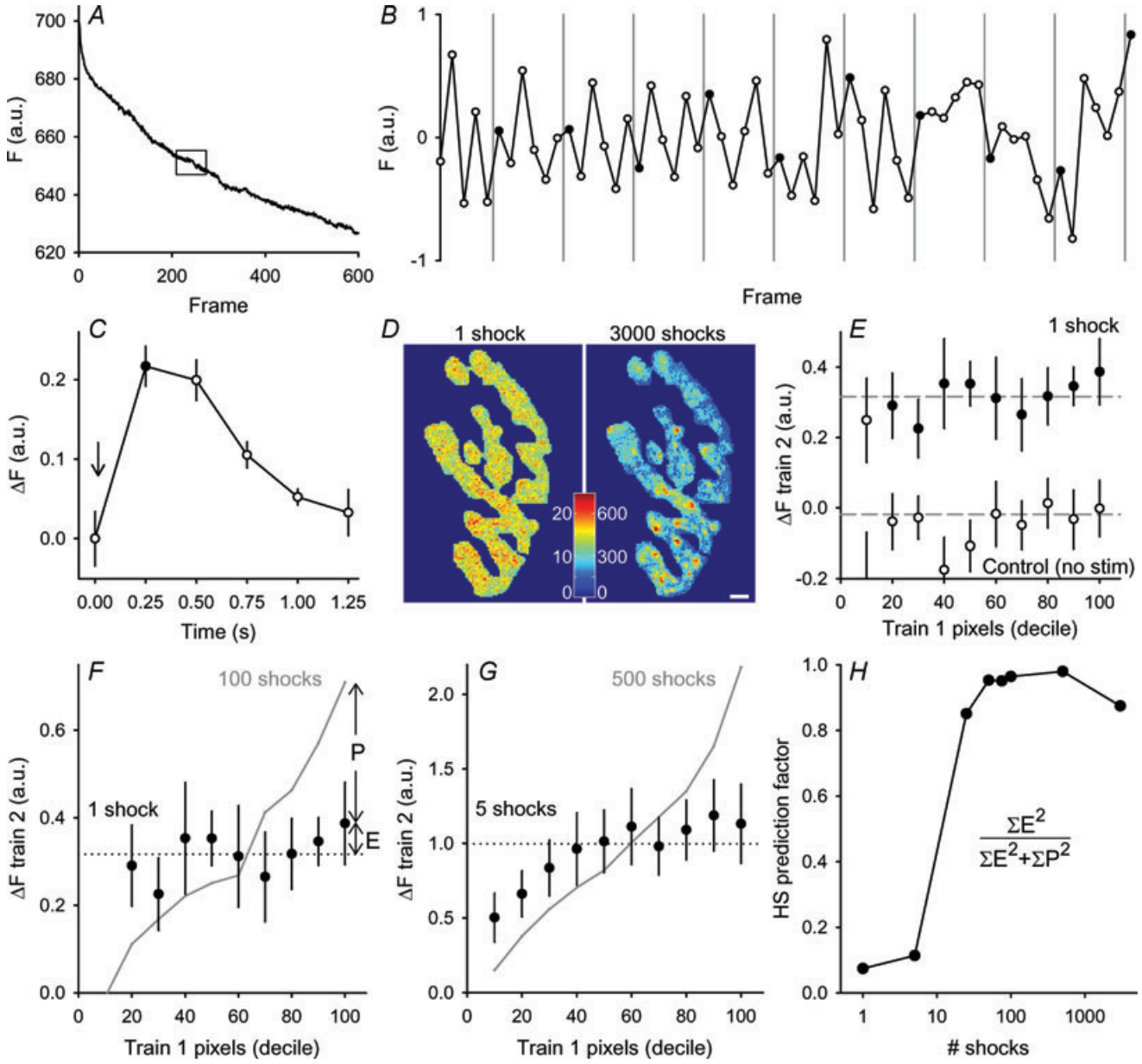

Figure 3. Locations of spH added during mild stimulation are not predicted by high frequency trains
A, raw fluorescence intensity (a.u.) for a single trial is plotted for each frame before photobleaching correction. *B*, boxed region shown in panel *A* corrected for photobleaching (see Methods) and plotted. Sixty frames are shown with each stimulation frame indicated by a filled circle. Shocks were delivered at points indicated by vertical grey lines. *C*, average fluorescence change (a.u.) is plotted versus time for a single shock. The six repeated frames were averaged for the 100 repeats in a trial. The shock was delivered at the arrow. Data represent an average of 8 trials. *D*, left: average fluorescence change in response to one shock (100 repeats at 0.67 Hz). Note the even colour distribution of mostly greens and yellows. Right: average fluorescence change in response to 3000 shocks at 100 Hz. Colour bar indicates fluorescence in a.u. Here the hot spots are clearly identifiable by the dark red colour. Scale bar = 3 μm. *E*, pixels were separated into deciles based on spH fluorescence changes after a 30 s, 100 Hz stimulation as in Fig. 1*D* (train 1). Those same locations were followed during a second stimulation of 100 shocks at 0.67 Hz. Filled circles indicate the average response to a single shock in each of the deciles. Open circles indicate the response in a control frame where no stimulation was delivered. The dashed lines are the terminal averages for either control or stimulation frames. The top nine deciles (or top 90% of spH increase in the terminal) showed a significant increase in fluorescence compared to controls ($P < 0.05$, Student's *t* test) while none of these nine deciles showed a significant difference from one another. $n = 13$ trials. *F* and *G*, similar plots to Fig. 2, but for one and five shocks, respectively. The deciles were determined as before. Train 2 is now an average of 100 trains of either one or five shocks (100 Hz) with each train separated by 1.5 s. Data are plotted as filled circles. The grey lines indicate the expected train 2 responses if 100 or 500 shocks were delivered at 100 Hz, then scaled down to

not arise from clustering of fusion sites (assuming these sites are identical and independent in their behavior – see Discussion). Otherwise, hot spot locations should have emerged from the averaged responses to one or a few stimuli.

Analysis of 'hot pixels' confirms the equal spatial distribution of release after mild stimulation

We next tried to identify specific sites of spH release in response to a single shock. Figure 4*A* shows responses of two exemplar pixels to repeated single shocks given every six frames (vertical lines). The obvious signal to noise problem prevented detection of any clear response to the shock. However, when the repeated six frames were averaged and plotted (Fig. 4*B*), the response to stimulation became quite visible.

We next tested whether we could identify these pixels as responding to multiple single shocks during a 100 shock run. We reasoned that, on average, the slope from one control frame to the next should have an equal probability of being positive or negative. However, a region that responds repeatedly to a single shock should be more likely to have positive slopes following stimulation. We calculated for each frame step the number of positive slopes as a fraction of the total (Fig. 4*C*). For example, 14 out of 17 (0.82) slopes were positive for the open symbols pixel going from frame 5 to frame 6 (Frame no. 6 on the *x*-axis). Overall, only the frame after stimulation (going from frame 5 to frame 6) rose more than 3 standard deviations above the mean positive slope fraction. We defined these pixels as 'hot pixels'. On account of the smoothing we performed for this analysis (see Methods), the areas identified (centred on a hot pixel) probably contained more than one fusion site (see Discussion).

We performed the same analysis on all of the pixels in many different terminals. As shown in Fig. 4*D*, control frames (filled circles) showed five to seven hot pixels, as expected (in a Gaussian distribution, 0.15% lie 3 standard deviations above the mean; terminals averaged about 4000 pixels, predicting about six hot pixels per terminal), while frames immediately following stimulation (open circles) showed significantly more (29, 43 and 201 hot pixels for one, two, and five shocks, respectively). We do not know precisely what these hot pixels represent, but presumably the majority of them reflect the most probable release sites.

Further analysis revealed two additional features of interest. First, we repeated runs of 100 stimuli at low frequency, and fewer than 2% of the hot pixel locations coincided from the paired runs ($n = 4$ terminals with at least two paired runs per terminal). Thus the hot pixel locations do not overlap from one trial to the next, suggesting a random process that caused some sites to rise above the noise. Second, we asked whether the hot pixel locations could predict release during high frequency trains. We measured the fluorescence response during a 30 s, 100 Hz train in the hot pixels identified as in Fig. 4*D* and compared this value to both the average fluorescence response to the whole terminal and to the pixels in the 100% decile (hot spots). Results, plotted in Fig. 4*E*, show that the fluorescence change in hot pixels is not different from the terminal average and considerably lower than the fluorescence change in the hot spots. We also observed a clear lack of spatial overlap between the hot spots and hot pixels (red and green, respectively, in Fig. 4*F*). Therefore, the release sites identified during low frequency stimulation could not predict the sites of most spH accumulation during a long, high frequency train. This confirms and extends the observation (Fig. 3) that hot spots do not predict release sites with mild stimulation, and *vice versa*.

Surface spH moves in the terminal membrane before endocytosis

Results presented above show that spH hot spots do not appear until after 5–25 shocks of high frequency stimulation, and that the locations of the hot spots are not correlated with low frequency release sites. While it is natural to think of the hot spots as exocytic in origin, both of these observations are also consistent with the hypothesis that hot spots mark sites of bulk endocytosis, a slower form of membrane retrieval involving relatively large infoldings of the surface membrane (Heuser & Reese, 1973; Richards *et al.* 2000; de Lange *et al.* 2003; Royle & Lagnado, 2003; Teng *et al.* 2007). In this scenario, after exocytosis, spH would be concentrated by transport processes at the hot spots as a prelude to slow reinternalization, resulting in a slower fluorescence decay at hot spots. To test this hypothesis, we first performed fluorescence recovery after photobleaching (FRAP) experiments to measure spH mobility in the

match average intensity levels for either one or five shocks (dotted lines). $n = 13$ trials for 1 shock and 11 trials for 5 shocks. *H*, hot spot (HS) prediction factor is plotted for each of the stimulation durations shown in Fig. 2 and panels *F* and *G*. HS prediction factor was calculated by comparing the observed result to both an equal distribution (E in panel *F*) and to that predicted by train 1 (P in panel *F*) for each decile. These differences were then squared, and summed for the top nine deciles using the equation shown. Note the number of shocks axis is plotted on a logarithmic scale.

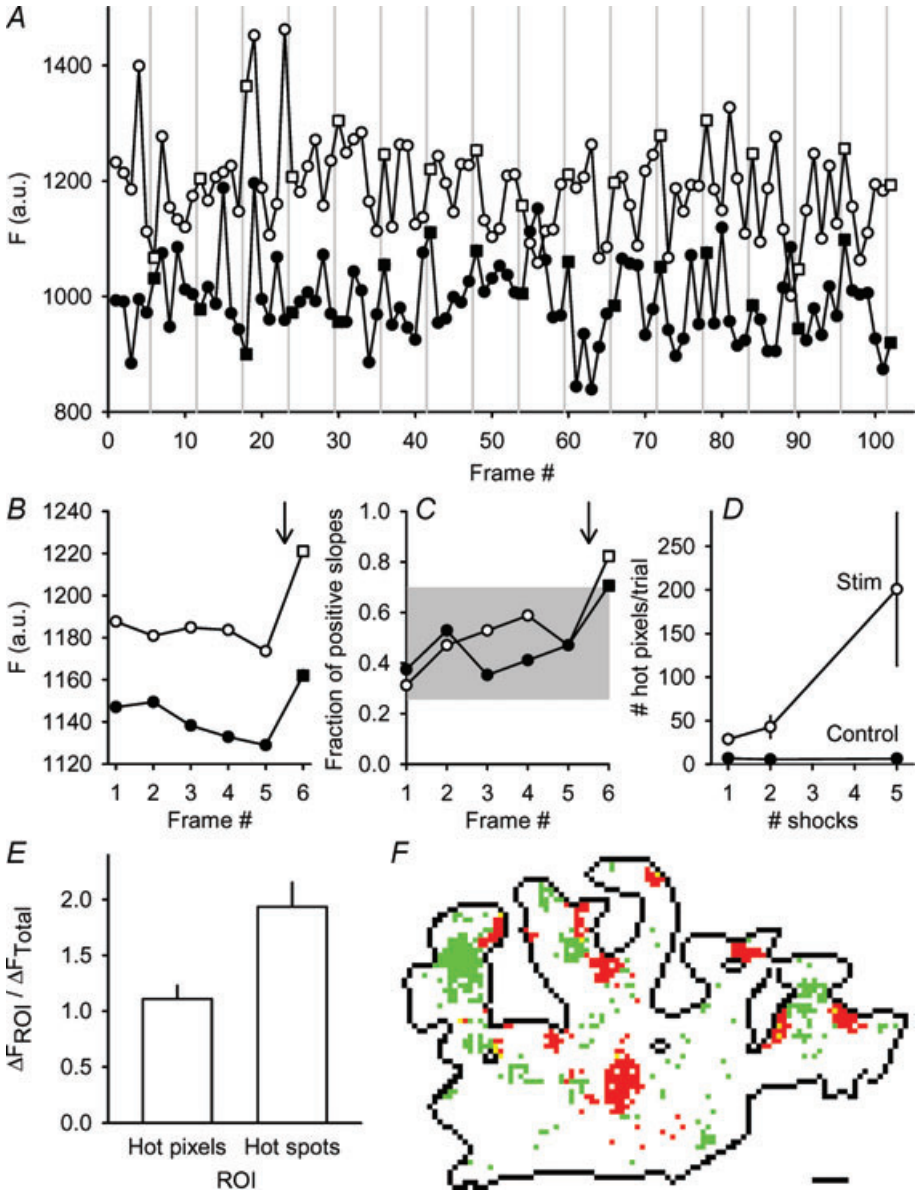

Figure 4. Locations of spH release from single shocks are not predictable
A, fluorescence (a.u.) is plotted for two different pixels for a subset of the total frames (4 Hz imaging rate). A single shock was delivered immediately before every sixth frame (vertical grey lines). Control frames are shown as circles and stimulation frames as squares. The filled symbol trace has been offset for clarity. *B*, fluorescence (a.u.) plotted for the same two pixels shown in panel *A*. The average response to the single shock (indicated by arrow) is apparent in frame 6. The filled symbol trace has been offset for clarity. *C*, the fraction of positive slopes to total trials is plotted for each frame for the two pixels in panel *A*. The grey area represents the space occupied by 3 standard deviations from the mean fraction of positive slopes. Only the frame immediately after the stimulation (arrow) lies outside of this region. These pixels were defined as hot pixels. Note that Frame 1 is the step from frame 6 to frame 1. *D*, number of hot pixels per terminal was averaged per trial and plotted for three different stimulation durations for hot pixels identified by either control (filled circles) or by stimulation frames (open circles). A significant number of hot pixels was found in the stimulation frames as compared to controls for 1 and 2 shocks ($P < 0.05$; Student's t test). Considerable variation prevented significance in the 5 shock data. $n = 11$, 7 and 8 trials for 1, 2 and 5 shocks, respectively. *E*, the fluorescence change during a 30 s, 100 Hz train was monitored in two different regions of interest (ROIs): hot pixels (identified as in panel *D*), and hot spots (as identified using the 100% decile from a prior 30 s, 100 Hz train). Results are plotted as a fraction of the average fluorescence change for the whole terminal (ΔF_{Total}). The average fluorescence change in identified hot pixels was slightly, but not significantly more than the terminal average (ratio $= 1.11 \pm 0.12$; $P = 0.198$, Student's t test). In contrast, the

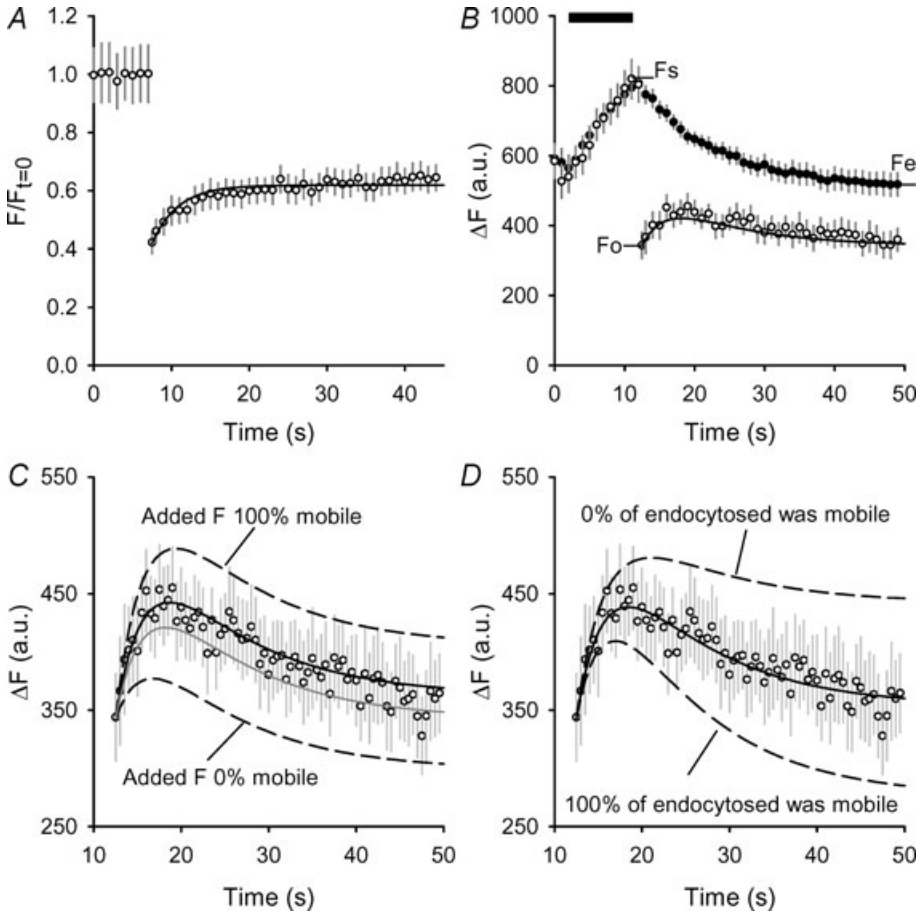

Figure 5. spH exocytosed during stimulation is mobile on the surface before being endocytosed
A, resting terminal FRAP. Average fluorescence as a fraction of initial level is plotted *versus* time. After 8 control images, a resting terminal was bleached then allowed to recover. The continuous line shows the single exponential best fit. The mobile fraction was 41.2 ± 5.3%. $n = 16$ trials. *B*, average fluorescence levels (arbitrary units, a.u.) are plotted over time. A 10 s, 100 Hz train (horizontal bar) was delivered after collecting control frames. A single, small (~2.25 μm diameter) circle in the terminal was bleached at the end of stimulation (region plotted as open circles) while the rest of the terminal was used as a control (filled circles). The expected recovery curve based on control data (panel *A*, see Methods) predicts the observed data with reasonable accuracy. Three parameters from eqn (1) (used to model recovery, see Methods) are also shown: F_s, fluorescence at end of stimulation; F_o, fluorescence in bleached region after bleach; F_e, fluorescence in unbleached region after completion of endocytosis and reacidification. $n = 11$ trials. *C*, data from panel *B* are plotted (open circles and grey line). A somewhat better fit (black line) is obtained by assuming that 60% of the added spH was mobile (as opposed to 41% from panel *A*). The dashed lines show the limits of the model. *D*, data from panel *B* (open circles) are plotted. The continuous line is the prediction based on 60% of added spH being mobile (cf. panel *C*), and 53% of the retrieved spH being from the mobile pool. While these modest changes improved slightly the quality of fit, the simplest assumptions of equal behaviour of surface and added spH, and indiscriminate retrieval of mobile and immobile spH seem probable. The dashed lines show the limits of the model.

surface membrane directly, and then compared rates of fluorescence recovery at hot spots and surrounding areas. Both types of experiments supported the hypotheses that hot spots are exocytic in origin. FRAP experiments by Tabares *et al.* (2007) found a small mobile fraction of surface spH at room temperature. As shown in Fig. 5*A*, we repeated and extended these studies, working at physiological temperature. A single exponential fit to the recovery

pixels identified as the 100% decile showed a significantly larger fluorescence change compared to the hot pixels (82.2 ± 25.9% more fluorescence; $P < 0.05$, Student's *t* test). $n = 6$ trials. *F*, terminal representative of typical hot spot and hot pixel locations. The terminal is outlined in black. Red pixels represent locations of the 100% decile (hot spots) and the green pixels represent hot pixel locations (collected from two runs each of 100 × 1, 100 × 2, and 100 × 5 shocks). Note the lack of overlay between hot spots and hot pixels (just a few yellow pixels). Scale bar = 2 μm.

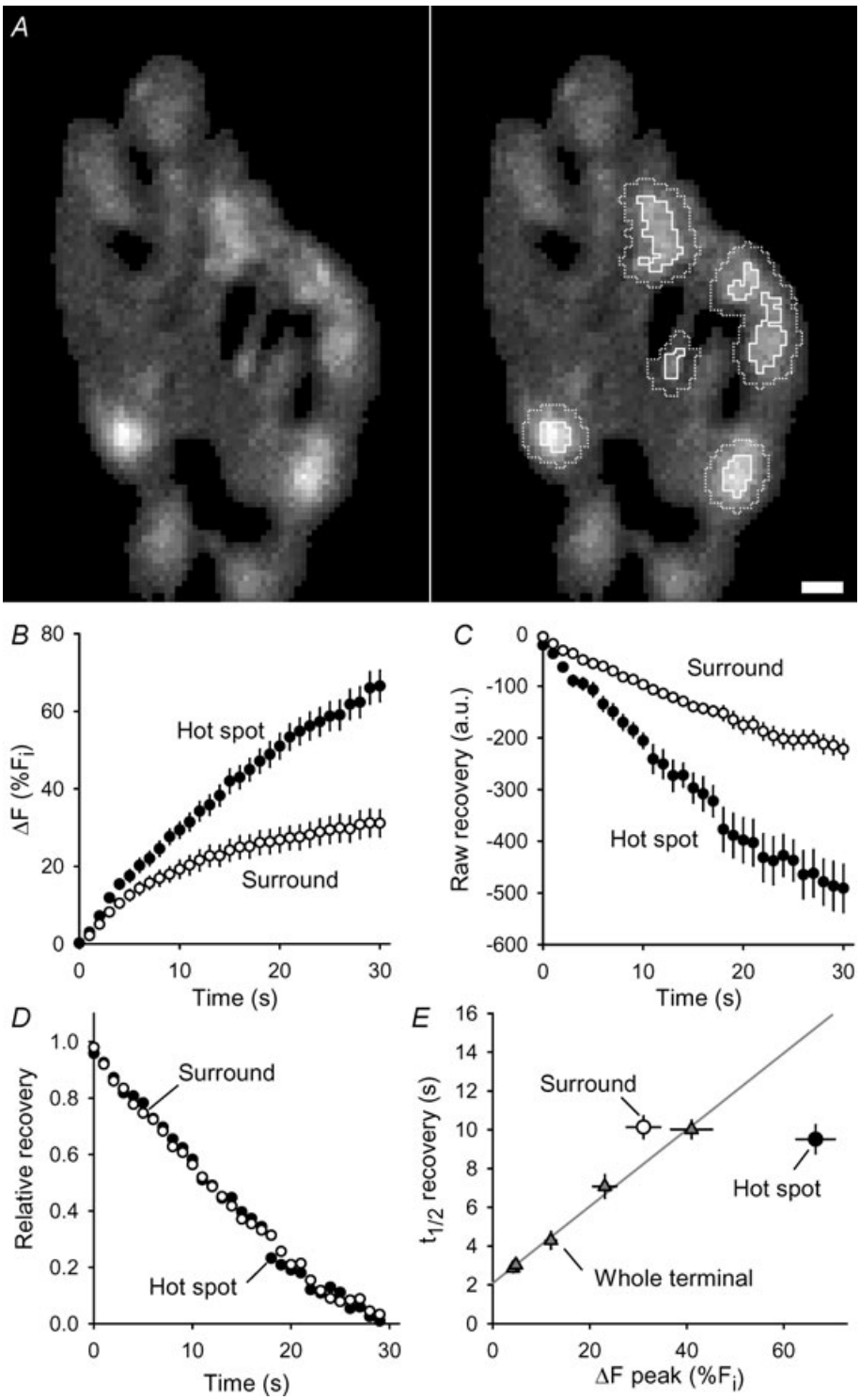

Figure 6. spH recovery is faster at hot spots and slower in surrounding areas
A, left: difference image showing the fluorescence change after a 30 s, 100 Hz stimulation. Right: hot spots are outlined with continuous lines, which enclose all pixels at least 75% as bright as the brightest pixel in the hot spot. Surrounds (dotted lines) outline regions three pixels from the edge of a hot spot yet still contained within the terminal. Scale bar = 2 μm. *B*, average fluorescence change as a percentage of initial fluorescence levels during a 30 s stimulus train (at 100 Hz) beginning at $t = 0$. For this and subsequent panels, filled circles mark hot spots and open circles mark surrounds. $n = 28$ spots from 5 terminals. *C*, raw fluorescence recovery (arbitrary units, a.u.) after stimulation for hot spots and surround are plotted versus time with stimulation ending at time = 0 and initial fluorescence levels set to 0. *D*, same as panel *C* except relative recovery is plotted as a fraction of total

indicated a 41% mobile fraction, a value somewhat higher than at room temperature (16%; Tabares *et al.* 2007), with a time constant of ∼3 s, and a diffusion coefficient of ∼0.5 $\mu m^2 s^{-1}$, similar to room temperature and typical for protein diffusion within membrane (Frick *et al.* 2007).

Because resting mobility may not necessarily indicate mobility of spH added by nerve stimulation, we next performed FRAP experiments when the bleach occurred immediately after stimulation (10 s, 100 Hz; Fig. 5*B*). Our bleaching protocol did not allow us to accurately identify hot spots before the bleach; therefore, we bleached small regions randomly selected throughout the terminal, expecting these regions to be representative of the entire terminal. Similarly, we assumed resting spH mobile fractions on the terminal surface to be consistent throughout the terminal. Before bleaching, fluorescence increased similarly in control regions (filled circles) and regions to be bleached after stimulation (open circles). After the bleach, control regions immediately began to recover as surface spH was internalized and reacidified. In bleached regions, however, fluorescence transiently increased, reflecting spH movement into the bleached areas. We used the resting terminal recovery curve (Fig. 5*A*) to predict FRAP recovery after stimulation (Fig. 5*B*, continuous line), assuming that the mobile fraction (0.41) of added spH was the same as control (see Methods). The reasonable agreement with the observed recovery (open circles) suggests that spH added by exocytosis behaves nearly the same as background spH in the resting terminal membrane.

The fit in Fig. 5*B* was not perfect, and we wondered if it could be improved. In Fig. 5*C*, the same data (open circles and grey line) are plotted. The dark line is a better fit to the data; it was drawn assuming that 60%, not 41% of the added spH was mobile. The dashed lines in Fig. 5*C* show the limits of the modelling. Finally, (Fig. 5*D*) we tried to discern whether endocytic mechanisms selectively recovered mobile or immobile spH. The best fit (continuous line) assumed that 53% of the recovered spH had been mobile on the surface (and, as in Fig. 5*C*, that 60% of the spH added during exocytosis was mobile). Dashed lines again show limits of the model. These are relatively small changes from that predicted by the simplest assumption, namely that preexisting surface spH and spH added during stimulation behave the same, and that endocytic mechanisms do not discriminate between mobile and immobile spH.

spH hot spots are not simply sites of bulk endocytosis

We next compared rates of fluorescence recovery within hot spots and within their immediate surround. Figure 6*A* shows the fluorescence change in response to a 30 s, 100 Hz train for a typical terminal (left panel) with several hot spots and their surrounds marked (right panel), which were determined as follows. We identified individual hot spots by eye, and then, using an automatic routine, mapped each hot spot (pixels in contact with the brightest pixel having at least 75% of its intensity) and its surround (pixels within 3 pixels of the hot spot edge). We then compared the fluorescence time courses for the hot spot and surround during stimulation and recovery. Figure 6*B* shows that hot spot fluorescence started to rise above the surround early during the train and continued to rise, even while the fluorescence in the surround had flattened. By the end of stimulation, over twice as much fluorescence existed within the hot spots compared to the surround. The raw recovery rates are shown in Fig. 6*C*; more absolute spH recovery occurred in the hot spot compared to the surround. However, the *relative* recovery rates (Fig. 6*D*) were nearly identical. If slower, bulk endocytic retrieval were occurring in the hot spot, we would have expected a slower relative recovery there. Finally, we compared fluorescence recovery half-times after different amounts of stimulation. As shown in Fig. 6*E* (triangles), the recovery half-time rose linearly with ΔF produced by stimulus trains (100 Hz) of different durations (linear regression slope = 0.2; intercept = 2.1s; $r^2 = 0.99$), as has been demonstrated before in cultured hippocampal neurons (Sankaranarayanan & Ryan, 2000, 2001) and mouse motor nerve terminals (Tabares *et al.* 2007). These measurements are whole terminal averages. However, the recovery half-times of hot spots alone (filled circle) were considerably faster, and the recovery half-times of hot spot surrounds alone (open circle) were slower than predicted from the whole terminal data. If the hot spots were simply sites of bulk endocytosis, then surface spH would have moved into the hot spots, slowing recovery. Instead this result suggests that fluorescence moved out of hot spots (speeding recovery there) into the surround (slowing recovery there). This is entirely consistent with the FRAP results (Fig. 5). Taken all together, these results suggest that spH hot spots are exocytic in origin, and that spH can diffuse into surrounding areas where it can be endocytosed.

fluorescence added during the stimulation. *E*, triangles show excellent linear relation between fluorescence recovery half times of whole terminals as a function of fluorescence change after different amounts of stimulation (50, 100, 200, 500 and 3000 shocks, from left to right, all at 100 Hz; $n > 5$ trials per duration). Data for hot spots (filled circle) show a faster recovery rate, while data from surrounds (open circle) show a slower recovery rate than predicted from whole terminal data (grey line).

Discussion

Our results show that exocytosis occurs preferentially at specific locations (hot spots), but only during intense stimulation; modest stimulation (1–5 shocks) evoked release uniformly from the entire terminal. Something happens after 5–25 shocks at high frequency to 'turn on' hot spots. This analysis is based on the assumption that fluorescence changes accurately reflect exocytosis of synaptic vesicles. Tabares *et al*. (2007) showed that with prolonged stimulation (more than 20 s at 100 Hz) fluorescence and electrophysiological (end plate potential (EPP) recordings) measures of release sometimes diverged, with summed EPPs lagging behind fluorescence. In the present work, however, signs of hot spots emerged early during a train (less than one second after the start), well before the divergence. Thus, it seems reasonable to conclude that in the present experiments fluorescence changes monitored synaptic vesicle exocytosis with reasonable fidelity. In addition, the emergence of hot spots so soon after the start of a train suggests that these findings are relevant to physiological levels of activity (Hennig & Lomo, 1985).

Several different mechanisms could account for hot spots; here we argue against three of them: synaptic vesicle clusters, access to different vesicle pools, and active zone clusters. In our previous experiments (Gaffield & Betz, 2007), the distribution of synaptic vesicles, as marked by FM1–43 uptake, was different from the hot spots. In particular, vesicles are more uniformly distributed; hot spots are generally much smaller than the groupings of vesicles. This is consistent with our observations that, at physiological temperature, most synaptic vesicles are diffusionally quite mobile (Gaffield & Betz, 2007), which would tend to disperse clusters. Vesicle mobility is much lower at room temperature, which could explain the results of Wyatt & Balice-Gordon (2008), who observed a positive correlation between spH hot spots and immunolabelled synaptic vesicles. Moreover, since recycling pool and reserve pool vesicles are spatially intermixed (Rizzoli & Betz, 2004), and 37°C mobilizes and facilitates vesicle mixing (Gaffield & Betz, 2007), hot spot locations likely do not have better access to recycling or reserve pools vesicles as compared to non-hot spot locations.

If we assume that all active zones behave in the same probabilistic way, then one might suppose that hot spots could arise from localized clusters of active zones. Our data from repeated single shocks, however, argue against this scenario, at least in its simplest form. If release is equally probable at each active zone, then the ∼70 vesicles that fuse during each shock, after averaging, should have revealed the clustered active zones as hot spots. Instead, it was impossible to discern hot spot locations from the uniform spatial pattern of release during single shock stimulation. This evident lack of clustered active zones is consistent with histological observations of bassoon (an active zone protein; tom Dieck *et al.* 1998) labelling in adult mouse motor nerve terminals, where punctate fluorescent dots appeared evenly distributed throughout the terminal rather than in clusters (Nishimune *et al.* 2004).

Release at non-active zone locations has been observed in ribbon-type synapses and might also contribute to the total spH signal we observed (Zenisek *et al.* 2000, 2003). In the case of ribbon-type synapses, non-active zone release accounted for one-third of total fusion events during ∼1 s long voltage steps (Zenisek *et al.* 2000); however, this same group later reported that fusion occurs outside of active zones at >100-fold lower rates per unit of terminal area than at active zones, and concluded that fusion is 'highly site-specific for active zones' (Zenisek *et al.* 2003). One important distinction between ribbon type synapses and conventional synapses like those we studied is the difference in active zone density; ∼0.1 per μm^2 in goldfish bipolar neurons (Zenisek *et al.* 2003) and ∼2.5 per μm^2 in mammalian motor nerve terminals (Fukunaga *et al.* 1983, 1987). This 25-fold difference might reduce the amount of non-active zone release in motor nerve terminals since synaptic vesicles are more likely to be near the specialized active zone machinery. Nevertheless, the possibility of non-active zone release during mild and heavy stimulation is an important area for future investigation.

If we assume that the majority of release does occur at active zones, then we propose that all active zones do not behave equally during high frequency stimulation. Some evidently can engage in reuse more than others, and those that can are not randomly spaced, but are grouped in clusters. It is not known whether the effect arises from spatial segregation of qualitatively different isoforms of channels, SNARE proteins, or some other key molecule, or from non-linearities that arise from groupings of otherwise identical molecules, such as calcium channels (or both). Further investigations might focus on pathways implicated in improved synaptic vesicle recruitment including cAMP (Sakaba & Neher, 2001*b*; Zhong & Zucker, 2005), myosin (Polo-Parada *et al.* 2005), actin (Sakaba & Neher, 2003), and CaMKII (Sakaba & Neher, 2001*a*). Additionally, active zones in hot spots may have more efficient re-priming of the SNARE proteins (Deak *et al.* 2006; Rizo & Rosenmund, 2008).

Working at 37°C, we found that fluorescence recovery occurred about three times faster than at room temperature (Tabares *et al.* 2007; cf. Renden & von Gersdorff, 2007; Balaji *et al.* 2008), reflecting perhaps slowed clathrin dynamics, as demonstrated for snake motor nerve terminals (Teng *et al.* 1999). Indeed, with single shocks, recovery time constants of less that 2 s were evident (Fig. 3*C*; cf. Renden & von Gersdorff, 2007), significantly faster than reported for cultured hippocampal nerve terminals at room temperature

(∼15 s for endocytosis, Granseth *et al.* 2006; ∼4 s for reacidification, Atluri & Ryan, 2006). This rapid recovery may reflect rapid internalization of surface spH in the so-called 'readily retrievable pool' (Fernandez-Alfonso *et al.* 2006; Wienisch & Klingauf, 2006) possibly triggered simultaneously with exocytosis. Additionally, the faster recovery at 37°C may reflect an increase in intraterminal calcium levels at higher temperature, a mechanism shown to play a role in increasing spontaneous vesicle fusion rates at physiological temperature in mouse motor nerve terminals (Katz *et al.* 1997; Gaffield & Betz, 2007). For this scenario, higher calcium influxes, possibly through L-type calcium channels (Perissinotti *et al.* 2008), would increase endocytic capacity (Sankaranarayanan & Ryan, 2001; Balaji *et al.* 2008).

Motor nerve terminals prominently show infoldings of the surface membrane following intense stimulation, from which membrane is retrieved by endocytosis and recycled as vesicles (Heuser & Reese, 1973; Richards *et al.* 2000; de Lange *et al.* 2003; Royle & Lagnado, 2003; Teng *et al.* 2007). We thought that such membranous movement might be revealed as spH hot spots, marking not sites of exocytosis, but rather sites of endocytosis. Measurements of FRAP (Fig. 5) and localized fluorescence recovery rates (Fig. 6) combined with the ordered decile gradients (Fig. 1*C*) strongly suggest that a net diffusive movement of spH molecules occurs out of, not into, the hot spots, revealing their exocytic origin. We found evidence for diffusion of spH in resting terminals and in terminals recovering from stimulation. Presumably, diffusion accounts for spH movement *during* stimulation as well; however, we cannot rule out a more ordered movement, during heavy activity, that traffics spH to specific sites and turns off immediately after stimulation ends. We consider this scenario unlikely because the terminal would have trafficked spH to endocytic sites during stimulation that did not maintain their endocytic preference after stimulation.

The surface diffusion of exocytosed spH creates difficulty in identifying sites of release to one or a few stimuli, because during the 250 ms exposure time that we needed to acquire a single image with appropriately low noise, spH molecules could diffuse over a distance of several pixels, blurring the sharp fluorescence peak that should occur at the instant of exocytosis. Using a different pHluorin construct might improve conditions. For example, in cultured hippocampal neurons, pHluorin attached to the vesicular glutamate transporter reduced surface pHluorin levels by an order of magnitude (Voglmaier *et al.* 2006; Balaji & Ryan, 2007), thus allowing a single fusion event to rise above the terminal background. The recently developed pHluorin fused to the vesicular acetylcholine transporter may provide similar advantages for the motor nerve terminal (Brauchi *et al.* 2008).

References

Angaut-Petit D, Molgo J, Connold AL & Faille L (1987). The levator auris longus muscle of the mouse: a convenient preparation for studies of short- and long-term presynaptic effects of drugs or toxins. *Neurosci Lett* **82**, 83–88.

Atluri PP & Ryan TA (2006). The kinetics of synaptic vesicle reacidification at hippocampal nerve terminals. *J Neurosci* **26**, 2313–2320.

Balaji J, Armbruster M & Ryan TA (2008). Calcium control of endocytic capacity at a CNS synapse. *J Neurosci* **28**, 6742–6749.

Balaji J & Ryan TA (2007). Single-vesicle imaging reveals that synaptic vesicle exocytosis and endocytosis are coupled by a single stochastic mode. *Proc Natl Acad Sci U S A* **104**, 20576–20581.

Brauchi S, Krapivinsky G, Krapivinsky L & Clapham DE (2008). TRPM7 facilitates cholinergic vesicle fusion with the plasma membrane. *Proc Natl Acad Sci U S A* **105**, 8304–8308.

de Lange RP, de Roos AD & Borst JG (2003). Two modes of vesicle recycling in the rat calyx of Held. *J Neurosci* **23**, 10164–10173.

Deak F, Shin OH, Tang J, Hanson P, Ubach J, Jahn R, Rizo J, Kavalali ET & Sudhof TC (2006). Rabphilin regulates SNARE-dependent re-priming of synaptic vesicles for fusion. *EMBO J* **25**, 2856–2866.

Fernandez-Alfonso T, Kwan R & Ryan TA (2006). Synaptic vesicles interchange their membrane proteins with a large surface reservoir during recycling. *Neuron* **51**, 179–186.

Fernandez-Alfonso T & Ryan TA (2004). The kinetics of synaptic vesicle pool depletion at CNS synaptic terminals. *Neuron* **41**, 943–953.

Frick M, Schmidt K & Nichols BJ (2007). Modulation of lateral diffusion in the plasma membrane by protein density. *Curr Biol* **17**, 462–467.

Fukunaga H, Engel AG, Lang B, Newsom-Davis J & Vincent A (1983). Passive transfer of Lambert-Eaton myasthenic syndrome with IgG from man to mouse depletes the presynaptic membrane active zones. *Proc Natl Acad Sci U S A* **80**, 7636–7640.

Fukuoka T, Engel AG, Lang B, Newsom-Davis J, Prior C & Wray DW (1987). Lambert-Eaton myasthenic syndrome: I. Early morphological effects of IgG on the presynaptic membrane active zones. *Ann Neurol* **22**, 193–199.

Gaffield MA & Betz WJ (2007). Synaptic vesicle mobility in mouse motor nerve terminals with and without synapsin. *J Neurosci* **27**, 13691–13700.

Gaffield MA, Rizzoli SO & Betz WJ (2006). Mobility of synaptic vesicles in different pools in resting and stimulated frog motor nerve terminals. *Neuron* **51**, 317–325.

Granseth B, Odermatt B, Royle SJ & Lagnado L (2006). Clathrin-mediated endocytosis is the dominant mechanism of vesicle retrieval at hippocampal synapses. *Neuron* **51**, 773–786.

Hennig R & Lomo T (1985). Firing patterns of motor units in normal rats. *Nature* **314**, 164–166.

Heuser JE & Reese TS (1973). Evidence for recycling of synaptic vesicle membrane during transmitter release at the frog neuromuscular junction. *J Cell Biol* **57**, 315–344.

Katz E, Protti DA, Ferro PA, Rosato S & Uchitel OD (1997). Effects of Ca^{2+} channel blocker neurotoxins on transmitter release and presynaptic currents at the mouse neuromuscular junction. *Br J Pharmacol* **121**, 1531–1540.

Kushmerick C, Renden R & von Gersdorff H (2006). Physiological temperatures reduce the rate of vesicle pool depletion and short-term depression via an acceleration of vesicle recruitment. *J Neurosci* **26**, 1366–1377.

Micheva KD & Smith SJ (2005). Strong effects of subphysiological temperature on the function and plasticity of mammalian presynaptic terminals. *J Neurosci* **25**, 7481–7488.

Miesenbock G, De Angelis DA & Rothman JE (1998). Visualizing secretion and synaptic transmission with pH-sensitive green fluorescent proteins. *Nature* **394**, 192–195.

Nishimune H, Sanes JR & Carlson SS (2004). A synaptic laminin-calcium channel interaction organizes active zones in motor nerve terminals. *Nature* **432**, 580–587.

Perissinotti PP, Giugovaz TB & Uchitel OD (2008). L-type calcium channels are involved in fast endocytosis at the mouse neuromuscular junction. *Eur J Neurosci* **27**, 1333–1344.

Polo-Parada L, Plattner F, Bose C & Landmesser LT (2005). NCAM 180 acting via a conserved C-terminal domain and MLCK is essential for effective transmission with repetitive stimulation. *Neuron* **46**, 917–931.

Renden R & von Gersdorff H (2007). Synaptic vesicle endocytosis at a CNS nerve terminal: faster kinetics at physiological temperatures and increased endocytotic capacity during maturation. *J Neurophysiol* **98**, 3349–3359.

Richards DA, Guatimosim C & Betz WJ (2000). Two endocytic recycling routes selectively fill two vesicle pools in frog motor nerve terminals. *Neuron* **27**, 551–559.

Rizo J & Rosenmund C (2008). Synaptic vesicle fusion. *Nat Struct Mol Biol* **15**, 665–674.

Rizzoli SO & Betz WJ (2004). The structural organization of the readily releasable pool of synaptic vesicles. *Science* **303**, 2037–2039.

Royle SJ & Lagnado L (2003). Endocytosis at the synaptic terminal. *J Physiol* **553**, 345–355.

Sakaba T & Neher E (2001*a*). Calmodulin mediates rapid recruitment of fast-releasing synaptic vesicles at a calyx-type synapse. *Neuron* **32**, 1119–1131.

Sakaba T & Neher E (2001*b*). Preferential potentiation of fast-releasing synaptic vesicles by cAMP at the calyx of Held. *Proc Natl Acad Sci U S A* **98**, 331–336.

Sakaba T & Neher E (2003). Involvement of actin polymerization in vesicle recruitment at the calyx of Held synapse. *J Neurosci* **23**, 837–846.

Sankaranarayanan S & Ryan TA (2000). Real-time measurements of vesicle-SNARE recycling in synapses of the central nervous system. *Nat Cell Biol* **2**, 197–204.

Sankaranarayanan S & Ryan TA (2001). Calcium accelerates endocytosis of vSNAREs at hippocampal synapses. *Nat Neurosci* **4**, 129–136.

Tabares L, Ruiz R, Linares-Clemente P, Gaffield MA, Alvarez de Toledo G, Fernandez-Chacon R & Betz WJ (2007). Monitoring synaptic function at the neuromuscular junction of a mouse expressing synaptopHluorin. *J Neurosci* **27**, 5422–5430.

Teng H, Cole JC, Roberts RL & Wilkinson RS (1999). Endocytic active zones: hot spots for endocytosis in vertebrate neuromuscular terminals. *J Neurosci* **19**, 4855–4866.

Teng H, Lin MY & Wilkinson RS (2007). Macroendocytosis and endosome processing in snake motor boutons. *J Physiol* **582**, 243–262.

Teng H & Wilkinson RS (2000). Clathrin-mediated endocytosis near active zones in snake motor boutons. *J Neurosci* **20**, 7986–7993.

tom Dieck S, Sanmarti-Vila L, Langnaese K, Richter K, Kindler S, Soyke A, Wex H, Smalla KH, Kampf U, Franzer JT, Stumm M, Garner CC & Gundelfinger ED (1998). Bassoon, a novel zinc-finger CAG/glutamine-repeat protein selectively localized at the active zone of presynaptic nerve terminals. *J Cell Biol* **142**, 499–509.

Voglmaier SM, Kam K, Yang H, Fortin DL, Hua Z, Nicoll RA & Edwards RH (2006). Distinct endocytic pathways control the rate and extent of synaptic vesicle protein recycling. *Neuron* **51**, 71–84.

Wienisch M & Klingauf J (2006). Vesicular proteins exocytosed and subsequently retrieved by compensatory endocytosis are nonidentical. *Nat Neurosci* **9**, 1019–1027.

Wood SJ & Slater CR (2001). Safety factor at the neuromuscular junction. *Prog Neurobiol* **64**, 393–429.

Wyatt RM & Balice-Gordon RJ (2008). Heterogeneity in synaptic vesicle release at neuromuscular synapses of mice expressing synaptopHluorin. *J Neurosci* **28**, 325–335.

Yang XF, Ouyang Y, Kennedy BR & Rothman SM (2005). Cooling blocks rat hippocampal neurotransmission by a presynaptic mechanism: observations using 2-photon microscopy. *J Physiol* **567**, 215–224.

Zenisek D, Davila V, Wan L & Almers W (2003). Imaging calcium entry sites and ribbon structures in two presynaptic cells. *J Neurosci* **23**, 2538–2548.

Zenisek D, Steyer JA & Almers W (2000). Transport, capture and exocytosis of single synaptic vesicles at active zones. *Nature* **406**, 849–854.

Zhong N & Zucker RS (2005). cAMP acts on exchange protein activated by cAMP/cAMP-regulated guanine nucleotide exchange protein to regulate transmitter release at the crayfish neuromuscular junction. *J Neurosci* **25**, 208–214.

Acknowledgements

We thank Steve Fadul for unfailing assistance, Dr Kristin Schaller for help with genotyping, Dr Guillermo Alvarez de Toledo and Dr Rafael Fernandez-Chacon for valuable comments, and Clinton Cave for useful discussions. This work was funded by grants from the National Institutes of Health (5 RO1 NS023466) and the Muscular Dystrophy Association (MDA4204). M.A.G. is supported by a National Institutes of Health research training grant (5 T32 NS007083).